Journal of Photochemistry and Photobiology A: Chemistry 229 (2012) 39–45

Contents lists available at SciVerse ScienceDirect

Journal of Photochemistry and Photobiology A: Chemistry

journal homepage: www.elsevier.com/locate/jphotochem

Antibacterial Ag–ZrN surfaces promoted by subnanometric ZrN-clusters deposited by reactive pulsed magnetron sputtering

O. Baghriche[a,d], J. Kiwi[b], C. Pulgarin[a], R. Sanjinés[c,*]

[a] Ecole Polytechnique Fédérale Lausanne, EPFL-SB-ISIC-GGEC, CH-1015 Lausanne, Switzerland
[b] Ecole Polytechnique Fédérale Lausanne, EPFL-SB-ISIC-LPI, CH-1015 Lausanne, Switzerland
[c] Ecole Polytechnique Fédérale Lausanne, EPFL-SB-IPMC-LPCM, CH-1015 Lausanne, Switzerland
[d] Laboratory of Innovative Techniques of Environment Preservation, Mentouri University, Constantine 25017, Algeria

ARTICLE INFO

Article history:
Received 1 May 2011
Received in revised form 8 December 2011
Accepted 10 December 2011
Available online 20 December 2011

Keywords:
Ag–ZrN-polyester
E. coli
Zr-promotion
Rugosity
TEM

ABSTRACT

Ag–ZrN films were deposited on polyester by direct current pulsed magnetron sputtering (from now on DCMSP) in Ar + N_2 atmosphere. ZrN on the polyester surface interacts with Ag leading to Ag–ZrN films. These composite films were more active in *Escherichia coli* inactivation compared to the Ag-films by themselves. The *E. coli* inactivation kinetics on Ag–ZrN polyester surfaces was accelerated >4 times compared to samples sputtering only Ag. Sputtering Zr in N_2 atmosphere presented no antibacterial activity by itself when applied for short times (< one min). The Ag–ZrN polyester sample sputtered for 20 s at 300 mA led to the fastest antibacterial *E. coli* inactivation kinetics within 11/2 h. This sample consisted of Ag-particles with sizes of 15–40 nm, within a layer thickness of 30–45 nm covering ~60–70% of the polyester fiber in the direction of the Ag^o/Ag-ion-flux from the Ag-target. An Ag sputtering time of 20 s lead to the optimal ratio of Ag-loading/Ag cluster size with the highest amount of Ag-sites held in exposed positions on the polyester surface. The Ag-nanoparticles sputtered for times >20 s agglomerated to bigger units leading to longer bacterial inactivation times. The Ag-atoms are shown to be immiscible with the ZrN-layer. The increase in thickness of the Ag–ZrN at longer sputtering times lead to a concomitant increase in rugosity and hydrophobic character of the Ag–ZrN sputtered layers. Several up-to date techniques have been used to characterize the catalytic Ag–ZrN film providing a full description of its structure. The Ag–ZrN films showed a uniform metal distribution and a semi-transparent gray-brown color.

1. Introduction

In the last decades, there has been increased interest in innovative antibacterial coatings due to the increasing resistance of pathogenic bacteria to synthetic antibiotics. This presents a serious problem for humans its associated high health care cost. Silver nanoparticles (NPs) have been reported as antimicrobial agents deposited in surfaces [1–10]. Recently magnetron sputtering has been used as an effective method of functionalizing cotton and polyester fabrics containing silver nanoparticles as *Escherichia coli* inactivation agent [11–15]. Also Ag films have been reported to prevent bacterial colonization of glass surfaces [16,17] prostheses and catheters [18], dental implants [19] and on several metal solid surfaces [20]. Ag-nanoparticles provide large area-to-volume ratio and high reactivity being used in healing pads/textiles [4–9]. The sputtering of Ag-leads to uniform thin films composed of nanocrystallites showing a high bactericide activity and adequate film adhesion [7,21].

Recently reports have appeared in the literature that some Ag or Cu based transition metal nitride (TmN) nanocomposites such as Ag–TiN and Ag–ZrN [22–25]. Me–TmN (Me = Ag, Cu, Pt) has been investigated for biological applications showing the formation of Ag–TmN bi-phased nanocomposites with separated Ag and cubic fcc-TmN nanocrystallites. This occurs due to the non-miscibility of the Ag atoms in the fcc-TmN phase due to the higher Ag-nitridation energy compared to the TmN formation energy.

We address in this study the experimental evidence for: (a) the bactericide role of Ag and ZrN (or Zr) in sputtered films of Ag–ZrN, (b) the role of Ag and Zr separately in the inactivation kinetics of *E. coli*, (c) the optimization for the integration of these two components into a hybrid sputtered film with high antimicrobial activity, (d) the detailed study of the Ag–ZrN film structure and (e) the correlation of DCMSP sputtered Ag-surfaces with the antibacterial kinetics, Ag–ZrN layer thickness, layer rugosity and hydrophobicity.

DCMSP has been used for the deposition of Ag–ZrN uniform, highly active and adherent films on polyester leading to *E. coli* inactivation. The development of high value added products such as the

* Corresponding author.
E-mail address: john.kiwi@epfl.ch (J. Kiwi).

1010-6030/$ – see front matter © 2011 Elsevier B.V. All rights reserved.
doi:10.1016/j.jphotochem.2011.12.004

Ag–ZrN investigated in this study focusing on bactericide textiles is increasing rapidly in the last few years [5,6,8,11–14].

The powder crystallite of Zr and Ag present sizes <100 nm being able to diffuse through biological cell-wall members. Although the magnetron sputtering is carried out in closed chambers one has to pay attention to the toxicology potential of these powders when handling these powders open to air.

2. Experimental

2.1. Materials and Ag–ZrN sputtering on polyester by DCMSP

Ag–ZrN deposited on polyester fibers by DCMSP using simultaneously targets of Ag (99.99 at.%) and Zr (99.98 at.%) in confocal configuration. The distance between the targets and the polyester substrate was 10 cm and the diameter of the targets was 5 cm. The residual pressure in the sputtering chamber was in the 5×10^{-5} Pa range. The working pressure ($Ar + N_2$) was 0.5 Pa and the reactive nitrogen partial pressure was fixed at 10% to obtain cubic ZrN. The deposition was performed at room temperature. The DCMSP Ag sputtering used two currents at 50 mA (20 W) and 300 mA (270 W) in order to change the Ag-content in the Ag–ZrN film. The DCMSP was operated at 50 kHz with 15% reversed voltage. The current on the Zr target fixed was 290 mA (100 W) whereas that of the Ag target was varied in the range 50–300 mA (20–270 W).

The polyester used was Dacron, type 54 spun, plain weave ISO 105-F04 used for color fastness determination. The nominal thickness calibration of the Ag–ZrN films as well as those of Ag and ZrN was carried out on Si-wafer. The film thickness was determined with a profilometer (Alphastep500, TENCOR).

2.2. X-ray fluorescence determination Cu-content on the cotton surface

The Ag- and Zr-content of the polyester was evaluated by X-ray fluorescence. By this technique, each element emits an X-ray of a certain wavelength associated with its particular atomic number and registered in a spectrometer RFX, PANalytical PW2400.

2.3. Bacterial inactivation of E. coli on Ag-polyester sputtered samples

The samples of *E. coli* K12 was obtained from the Deutsche Sammlung von Mikroorganismen und Zellkulturen GmbH (DSMZ) ATCC23716, Braunschweig, Germany to test the antibacterial activity of the Ag–ZrN-polyester fabrics. The polyester fabrics of 4 cm^2 square were sterilized by autoclaving at 121 °C for 2 h. The 20 μL aliquots of the culture with an initial concentration of 3.8×10^6 CFU mL^{-1} in NaCl/KCl were placed on each coated and uncoated (control) polyester fabric. The samples were placed on Petri dish provided with a lid to prevent evaporation. After each determination, the fabric was transferred into a sterile 2 mL Eppendorf tube containing 1 mL autoclaved NaCl/KCl saline solution. The concentration of NaCl is 8 g/L and of KCl is 0.8 g/L. The cell suspensions were diluted with a saline solution with 0.75% NaCl and KCl 0.08% to allow the storage of the bacteria without osmotic stress. This solution was subsequently mixed thoroughly using a Vortex for 3 min. Serial dilutions were made in NaCl/KCl solution. A 100-μL sample of each dilution was pipetted onto a nutrient agar plate and then spread over the surface of the plate using standard plate method. Agar plates were incubated, lid down, at 37 °C for 24 h before colonies were counted. The experimental points reported were a result of three individual experiments. To test the total absence of *E. coli* at the end point of the bacterial deactivation we spread 100 μL of the incubated bacterial solution for 24 h at 37 °C on three Petri dishes PCA and incubated these dishes for 24 h. The results confirmed the total absence of bacteria.

Table 1
Nominal thickness of Ag-coatings on Si-wafers sputtered by DCMSP at 50 mA and 300 mA.

Samples (DCP)	Time (s)	Thickness (nm)
Ag 50 mA	2	0.35
	5	0.875
	10	1.75
	20	3.5
	80	14
	320	56
	600	105
Ag 300 mA	2	3
	5	7.5
	10	15
	20	30
	80	120
	320	480
	600	900

2.4. Transmission electron microscopy of Ag-polyester samples

A Philips CM 12 (field emission gun, 300 kV, 0.17 nm resolution) microscope at 120 kV was used to measure the particles size of the Ag-nanoparticles. The polyester embedded in epoxy resin 45359 Fluka and the fabrics were cross-sectioned with an ultramicrotome (Ultracut E) and at a knife angle at 35°. Images were taken in Bright Field (BF) mode for the sputtered samples.

2.5. Atomic force microscopy (AFM)

The surface morphology was investigated using an UHV VT SPM (Omicron) working in noncontact mode (needle sensor).

2.6. Contact angle measurements

The contact angle of polyester and sputtered Ag–ZrN as a function of sputtering time were measured by means of a DataPhysics OCA 35 instrument following the Sessile's method for the analysis of water droplets by this technique.

2.7. XPS measurements

An AXIS NOVA photoelectron spectrometer (Kratos Analytical, Manchester, UK) equipped with monochromatic Al K_α ($h\nu$ = 1486.6 eV) anode was used during the study. The electrostatic charge effects on the samples were compensated by means of the low-energy electron source working in combination with a magnetic immersion lens. The carbon C 1s line with position at 284.6 eV was used as a reference to correct the charging effect. The quantitative surface atomic concentration of some elements was determined from peak areas using sensitivity factors. Spectrum background was subtracted according to Shirley (see Ref. [4]). The XPS spectra were analyzed by means of spectra deconvolution software (CasaXPS-Vision 2, Kratos Analytical UK).

3. Results and discussion

3.1. Thickness of the Ag-sputtered films on polyester and film Ag and Zr-content

The values of the thicknesses of the Ag-film as a function of DCMSP sputtering time at 300 mA is shown in Table 1 up to 600 s. Fig. 1 indicates that when using a current of 300 mA a

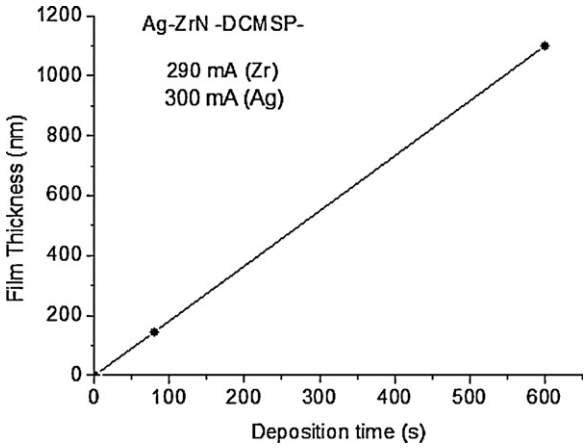

Fig. 1. Calibration of Ag in the Ag–ZrN film sputtered at 300 mA for Ag and 300 mA for Zr on Si-wafers.

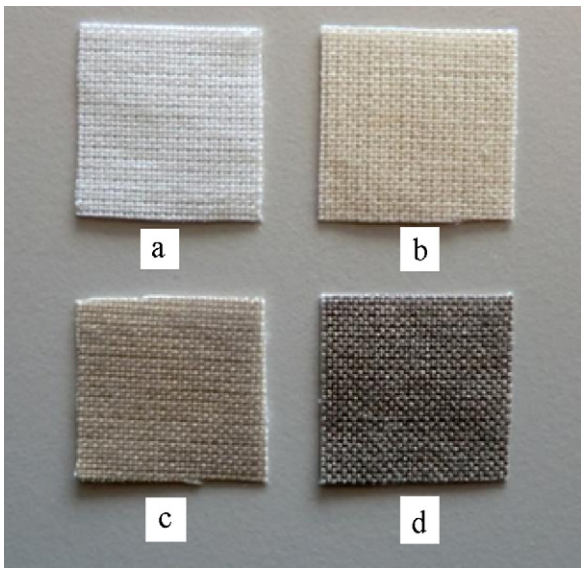

Fig. 2. Visual appearance of Ag–ZrN polyester sputtered under different experimental conditions: (a) polyester alone, (b) DCMSP AgZr–N films 10 s at 50 mA, (c) DCMSP AgZr-N films 2 s at 300 mA, and (d) DCMSP AgZr–N films 20 s at 300 mA.

thickness of 180 nm was attained after 80 s. The standard deviation in Fig. 1 for the Ag–ZrN layers calibrated on Si-wafers was ±10%. Within 1 s 1.2–1.25 nm film Ag was deposited equivalent to ~6 layers of 0.2 nm each leading to a rate of Ag deposition of 6×10^{15} atoms/cm^2 s. Taking the lattice distance of 0.3 nm between Ag-atoms. In this way an Ag-surface density of about 10^{15} atoms/cm^2 can be estimated.

The Ag- and Zr-content of the polyester sputtered samples was determined by X-ray fluorescence. Table 2 shows that the Ag-content as a function of sputtering time at 50 mA was low for Ag and only increased toward 20 s. For Zr, the values found were almost constant or below the detection level of the instrument of 0.0010% Zr (w/w) polyester. An increased Ag-deposition was attained sputtering at 300 mA up to 20 s, depositing about 8 times more Ag 20 s than when 50 mA was used. This is not surprising since at higher energies (currents) as applied by DCMSP a higher density flux of metal-ions/metal nanoparticles with energies >10 eV and up to 100 eV has been reported recently by Lin et al. [26].

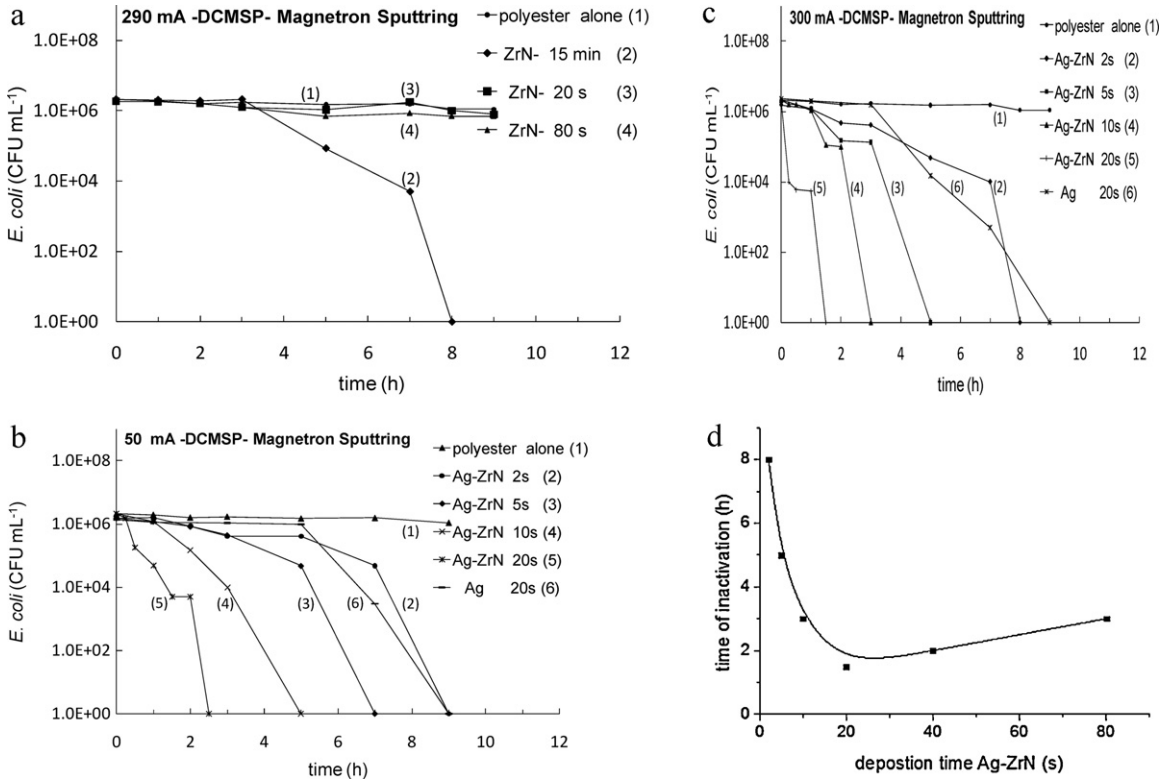

Fig. 3. (a) *E. coli* inactivation prepared by polyester by direct current magnetron sputtering (pulsed) for different times with Zr in Ar + 10% N_2 0.5 Pa atmosphere. (b) *E. coli* inactivation prepared by polyester confocal direct current magnetron sputtering (pulsed) for different times using an Ag- and Zr-target in (Ar + 10% N_2 0.5 Pa) atmosphere at 50 mA. (c) *E. coli* inactivation prepared by polyester confocal direct current magnetron sputtering (pulsed) at different times using an Ag- and Zr-target in (Ar + 10% N_2 0.5 Pa) atmosphere at 300 mA e. (d) Inactivation time of *E. coli* on Ag–ZrN polyester as a function of the deposition time by DCMSP sputtered at 300 mA.

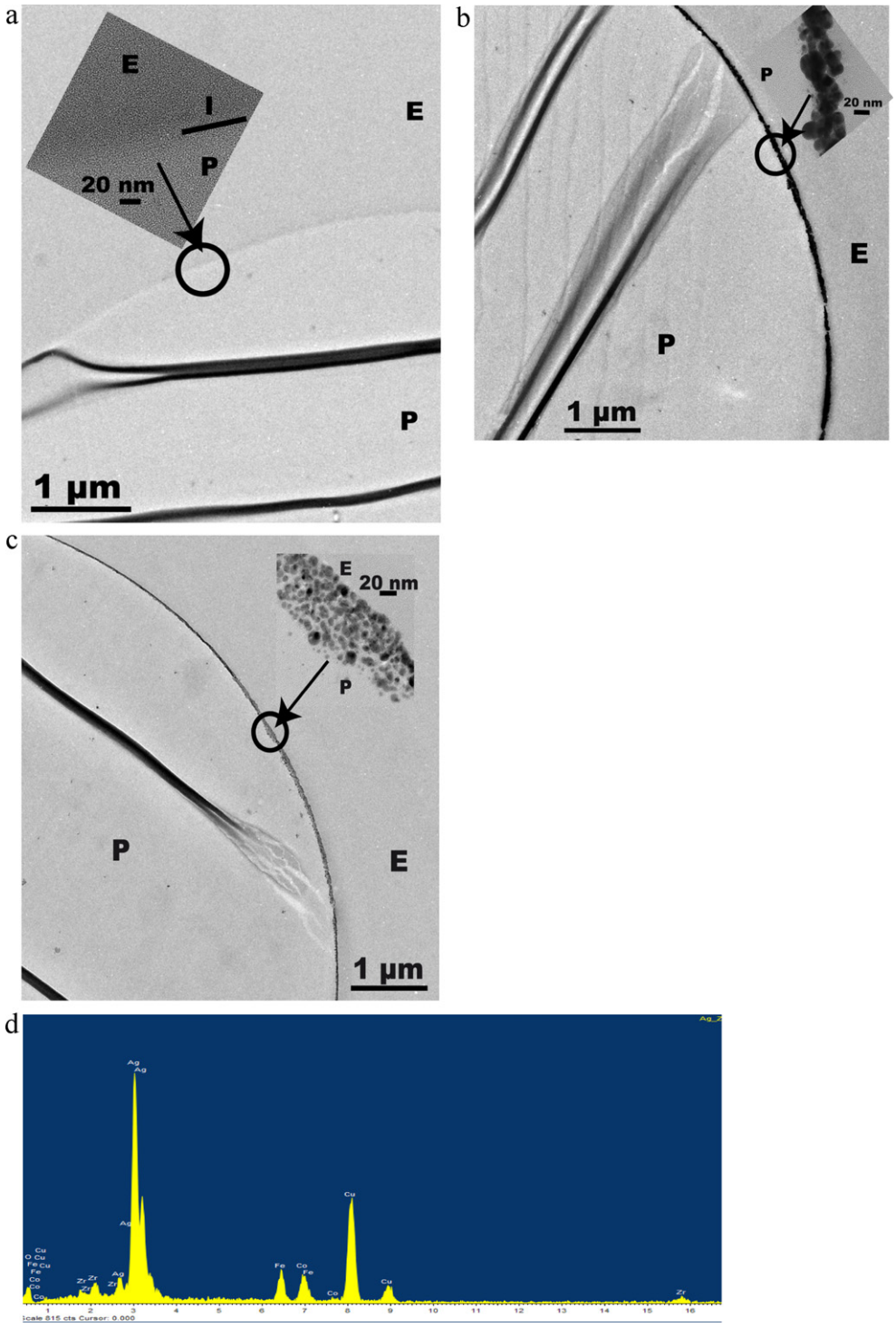

Fig. 4. (a) TEM of polyester fiber. E stands for the epoxide used to enrobe the fiber during the sample preparation and P stands for polyester. For other details see text. (b) TEM of a polyester P fiber cut at an angle of 35° embedded in an epoxy resin €, sputtered confocally for 5 s with Ag and Zr in an Ar + 10% N_2 0.5 Pa atmosphere. (c) TEM of a polyester (P) fiber cutat an angle of 35° embedded in an epoxy resin €, sputtered confocally for 20 s with Ag and Zr in an Ar + 10% N_2 0.5 Pa atmosphere. (d) EDS spectra of Ag–ZrN polyester for a sample sputtered 20 s at 300 mA.

3.2. Ag-films visual appearance as a function of sputtering time

The polyester alone in Fig. 2a shows no color in the absence of Ag–ZrN. A light gray-color appears in sample (b) indicative of Ag clusters/nanoparticles deposited at 50 mA for 10 s, (c) shows a darker-gray metallic Ag-color due DCMSP applied 2 s at 300 mA and finally (d) shows a dark mostly Ag-deposit on the Ag–ZrN-polyester sputtered for 20 s at 300 mA. (For interpretation of the references to color in the text, the reader is referred to the web version of the article.) The Ag-atoms diffuse anisotropically on the polyester surface [27] and the migration/aggregation of the Ag-particles is driven by the sputtering energy leading to thermodynamically stable agglomerates [28]. The color in Fig. 2d corresponds to the Ag_2O/Ag^o with a band-gap (b_g) 0.7–1.0 eV. This allows for an absorption edge up to about 1000 nm for the silver deposited on the polyester [29]. The strong preference for Ag binding other Ag-atoms rather than

Table 2
X-ray fluorescence determination of percentage weight Zr and Ag per weight polyester in DCMSP sputtered Zr–AgN polyester.

Sample Ag–ZrN polyester	Time (s)	wt% Ag/wt polyester	wt% Zr/wt polyester
50 mA	2	0.0010	0.0010
	5	0.0010	0.0010
	10	0.0010	0.0010
	20	0.0012	0.0010
300 mA	2	0.0018	0.0010
	5	0.0020	0.0010
	10	0.0067	0.0011
	20	0.0105	0.0012

polyester as the sputtering is applied for longer times leads to the formation of Ag-clusters. These clusters have been reported to be initially compact but no necessarily crystalline and are responsible for to the darkening of Ag-film as a function of sputtering time (Fig. 2) [30].

3.3. *E. coli* bacterial inactivation kinetics

Fig. 3a presents the *E. coli* inactivation kinetics when Zr was sputtered in an $Ar + N_2$ (0.5 Pa) atmosphere on polyester. When applying sputtering times of a few seconds no the bacterial inactivation was observed and by TEM analysis revealed no Zr-particles. These Zr-particles therefore had sizes <1 nm. Subnanometric particles of Fe and other metals presenting catalytic effects have been reported by our laboratory effective in the degradation of organic compounds [31,32]. Only the ZrN samples sputtered for 15 min presented bactericide properties. This observation will be discussed in the context of the results presented for the inactivation of *E. coli* by the Ag–ZrN-polyester in Fig. 3b–d.

Fig. 3b presents the experimental results for polyester coated by Zr and Ag confocal sputtering in $Ar + N_2$ atmosphere for 2 s, 5 s, 10 s and 20 s with at 50 mA. It is readily seen that polyester alone has no bactericide action and that the *E. coli* inactivation kinetics becomes faster at longer sputtering time due to the increased Ag-particle density attained with longer sputtering times. Trace (6) shows that when Ag is sputtered alone for 2 s, 9 h were necessary to inactivate *E. coli* compared to a 2.5 h inactivation period observed when Ag and Zr were sputtered simultaneously for 20 s at 50 mA. Fig. 3b shows that Ag–ZrN polyester samples containing a ZrN nanocomposite with Ag are more effective in *E. coli* inactivation compared to the Ag-nanoparticles by themselves.

Fig. 3c presents the faster inactivation kinetics attained by Ag/Zr targets applying currents of 300 mA. Fig. 3c shows an *E. coli* inactivation time of 1.5 h on Ag/Zr polyester sputtered for 20 s. The profile of trace (5) in Fig. 3c indicates that *E. coli* inactivation is a complex process. We suggest that this sample had the optimal ratio of Ag-loading/Ag cluster size with the highest amount of Ag-sites held in exposed positions active in the *E. coli* inactivation process. Table 2 indicates that the amount of Ag sputtered at 20 s was ~8 times higher applying 300 mA compared to 50 mA. Ag sputtered alone as a control experiment in Fig. 3c indicates an *E. coli* inactivation time of ~9 h. This shows the favorable effect of the ZrN during on the Ag-clusters during bacterial inactivation process.

Fig. 3d shows that for samples sputtered above 20 s, the *E. coli* inactivation kinetics became larger compared to samples sputtered for 20 s. The Ag-agglomerates becomes bigger but the catalytic activity per exposed atom decreased due to the Ag-agglomeration process. At times below 20 s, there was not enough Ag on the polyester to mediate the *E. coli* inactivation as shown in Table 2 by the X-ray fluorescence data.

The Ag-polyester samples are shown to lead to significant bacterial inactivation a shown in Fig. 3a–c. We suggest that the ROS of

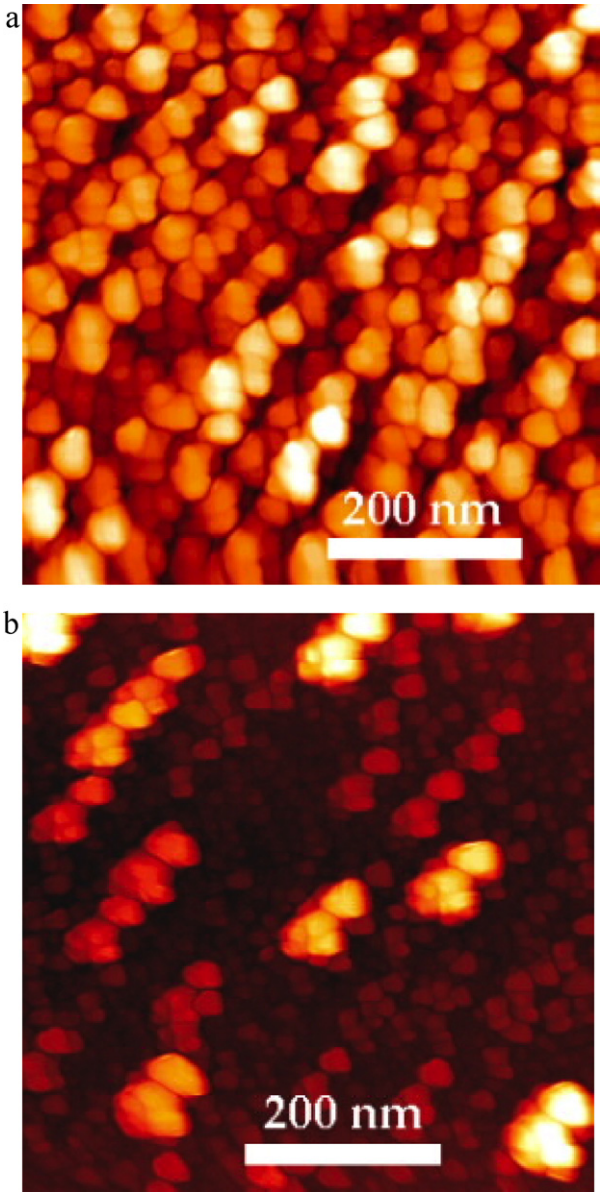

Fig. 5. (a) AFM image 600 nm × 600 nm of Ag–ZrN on Si-wafers sputtered at 300 mA for 2 s. (b) AFM image 600 nm × 600 nm of Ag–ZrN on Si-wafers sputtered at 300 mA for 20 s.

E. coli were modified by interaction with Ag^+/Ag^o by the reactions (1) and (2):

$$Ag^o + O_2 \rightarrow Ag^+ + O_2^{\bullet -} \quad (1)$$

$$Ag^+ + O_2^{\bullet -} \rightarrow Ag^o + O_2 \quad (2)$$

since H_2O_2 adsorbs on Ag/Ag_2O, peroxide decomposition may take place [6–8]:

$$H_2O_2 + Ag^o \rightarrow HO^- + OH^o + Ag^+ \quad (3)$$

3.4. Transmission electron microscopy of AgZr–N polyester samples

Fig. 4a presents the electron microscopy (TEM) of polyester. A bar-marker of 0.8 cm denotes the 20 nm scale in the insert. No nanoparticles were observed on the polyester fiber.

Fig. 4b shows the TEM of an Ag–ZrN polyester sample sputtered for 5 s at 300 mA. In Fig. 4b, the Ag-particles were 10–20 nm

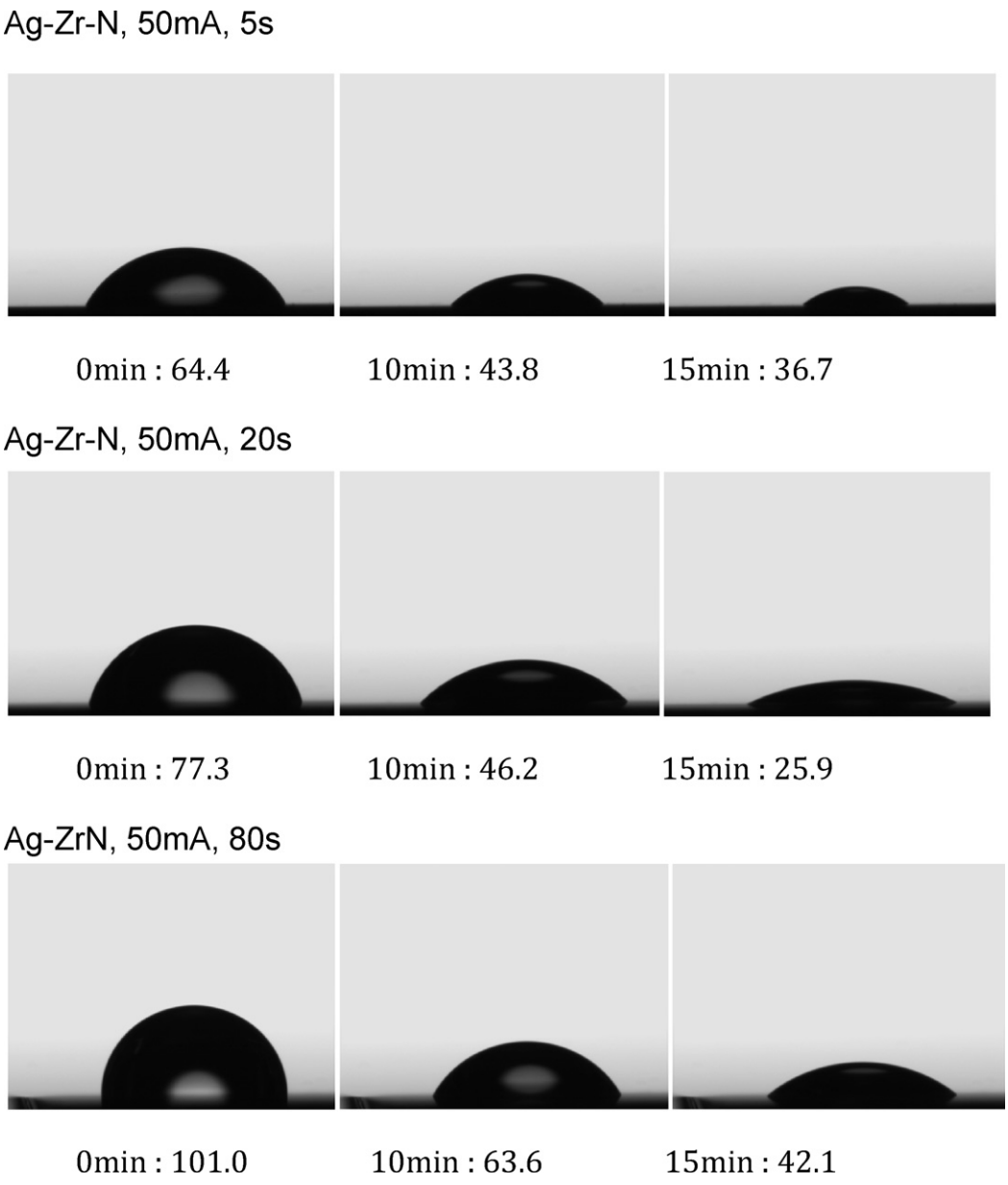

Fig. 6. Contact angle (CA) for Ag–ZrN polyester sputtered at 50 mA for 5, 20 and 80 s. For other details see text.

in diameters. Silver metallic particles have been reported to form above one nm [30]. The arrow in the upper right hand side in Fig. 4b shows the Ag^o/Ag-ions flux direction reaching the polyester fiber. Coverage of 60–70% of the polyester fiber was observed in the direction of the flux of the Ag^o/Ag-ions arriving from the Ag-target.

Fig. 4c shows the EM of an Ag–ZrN polyester sample sputtered for 20 s at 300 mA. The Ag-particles presented diameter sizes of 15–40 nm and were appreciably bigger compared to the Ag-nanoparticles sputtered for 5 s a shown in Fig. 4b. This shows that Ag-aggregates are formed in a process due to Ag growing on other Ag-particles rather than interacting with ZrN. This suggests immiscibility of the Ag-particles with small ZrN crystallites on the polyester surface. A continuous deposit 30–45 nm thick of metallic Ag-particles were observed and a silver coverage of ~60–70% of the polyester fiber in the direction of the Ag^o/Ag-ion-flux from the Ag-target.

Fig. 4d presents the electron diffuse spectroscopy (EDS) for the A-ZrN polyester sample sputtered for 20 s at 300 mA. The Cu-signals originate from the Cu-grid used as a support the EM sample. The Ag-peaks are seen to be more significant than the Zr-peaks, since its abundance of this element is much higher than Zr as shown in Table 2.

3.5. Atomic force microscopy of Ag–ZrN polyester sputtered at different times (AFM)

Fig. 5 shows 600 nm × 600 nm AFM images recorded on Ag–ZrN films sputtered on Si-substrates for 2 s and 20 s with 300 mA. The surface of the 2 s sputtered Ag–ZrN film in Fig. 5a is characterized by the presence of dispersed small crystallites of <20 nm in diameter and some large clusters >20 nm. The surface morphology of the 20 s sputtered Ag–ZrN film shown in Fig. 5b is qualitatively different from the film sputtered for 2 s. Irregular crystallites of different sizes (20–60 nm) are observed. These crystallites are well separated each other and the surface coverage is not homogenous as it is noticed from the large contrast in the z-scale. The crystallites are assigned to Ag, as the amount of ZrN is low and their size <1 nm as described in Fig. 4. The ZrN films on polyester are amorphous.

With increasing the deposition time, the film thickness was seen to increase (Table 1). The increase in thickness brings an increase in the surface roughness. The root mean square (rms) values changes with increasing sputtering times 1.8 μm at 5 s to 2.8 μm at 2 s and 3.2 μm at 80 s.

3.6. Contact angle measurements (CA)

Fig. 6 presents the contact angle for different Ag–ZrN samples on Si-wafers. No polyester was used for the contact angle measurements since the water droplet penetrated too quickly into the polyester and disappeared almost entirely at zero time. Samples sputtered for 5 s at 50 mA presented a contact angle of 64.4° at time zero. This contact angle decreased with the contact time on the Si-wafer surface due to the hydrophilic OH groups present on the Si-wafers. The Ag–ZrN sputtered Si-wafers become more hydrophobic after 20 s sputtering time as seen in the second rows showing an initial contact angle of 73.3°. Finally a contact angle of 101° was observed at time zero for 80 s sputtered samples. These samples were more hydrophobic due to the higher amount of Ag on the Si-wafers.

The increase in surface layer thickness and droplet contact angle or hydrophobicity is concomitant with an increase of surface layer roughness of the sputtered Ag-layers. We have recently identified the active Ag-ions active on Ag-layers responsible for *E. coli* inactivation [7]. A 20 s DCMSP sputtered sample presented a higher number of Ag-layers with a concomitant higher rugosity compared to samples sputtered for 2 s. This leads to a faster *E. coli* inactivation time as shown in Fig. 3a and b.

3.7. X-ray photoelectronic spectroscopy of Ag–ZrN polyester surfaces (XPS)

The percentage atomic concentration at time zero for polyester alone were: C 1s 76.4% and for O 1s 23.6%. Due to the DCSMP-sputtered Ag and Zr after 2 s the percentage atomic concentration changed to C 1s 60.6%, O 1s 23.6%, Ag 3d 13.6% and Zr 3d 2.1%. At 20 s sputtering, the percentage atomic concentration showed a significant increase in the Ag topmost 10 layers, with values: C 1s 23.4%, O 1s 10.6%, Ag 3d 63.6% and Zr 3d 2.5%. The Ag 3d5/2 peak was found at 368.1 eV [33]. The charge effects compensation was carried out according to Shirley [34]. Zr 3d5/2 peaks were detected at BE of 182 eV for the 2 s and also the 20 s Ag–ZrN samples corresponding to zirconia [35]. ZrO_2 appears when the Zr in the Ag–ZrN is exposed to air (O_2). Zirconia IR peaks at ~500 cm^{-1} were found for Zr-cluster sizes ≤6 Å have recently been reported [35]. No signal for N— was detected in the topmost 10 layers (2 nm) by XPS on the polyester surfaces indicating that the amounts found were below the detection limit for N— in the XPS spectrogram. In Fig. 4b and c the Zr was not detected since the limit of resolution by the TEM employed was ~1 nm. The Zr 3d5/2 peak was detected for the 2 s and the 20 s Ag–ZrN sputtered samples corresponding to zirconia at BE 182 eV [35]. ZrO_2 appears when the Ag–ZrN on the polyester was exposed to air (O_2). The zirconia IR peak at ~500 cm^{-1} with cluster sizes ≤6 Å has recently been reported [35].

4. Conclusions

- A sputtered Zr-promoted polyester coated with Ag–ZrN led to a faster *E. coli* bacterial inactivation compared with an Ag–N surface.
- Higher energies (currents) of 300 mA used during the confocal Ag–ZrN sputtering on polyester led to a higher Ag-deposition compared with 50 mA currents having beneficial effect on the antibacterial *E. coli* inactivation time.
- Ag–ZrN film sputtered at 300 mA for 20 s was able to inactivate *E. coli* within 11/2 h.
- This study presents the first experimental evidence relating the thickness of the Ag–ZrN layer to the Ag-grain sizes, the hydrophobic and roughness properties of the Ag–ZrN film. These properties are shown to be controlling parameters affecting the observed *E. coli* inactivation kinetics.

Acknowledgments

We wish to thank the COST Action MP0804 Highly Ionized Pulse Plasma Processes (HIPIMS), the EPFL and the Swiss-Hungarian Cooperation Program "Sustainable fine chemical pharmaceutical industry: screening and utilization of liquid wastes" for the support of this work.

References

[1] C. Gunawan, W. Teoh, P. Marquis, J. Lifia, R. Amal, Small 5 (2009) 341–344.
[2] K. Holt, A. Bard, Biochemistry 44 (2005) 13214–13223.
[3] A. Nel, T. Xia, L. Mädler, N. Li, Science 311 (2006) 622–627.
[4] S.H. Jeong, S.Y. Yeo, S.C. Yi, J. Mater. Sci. 40 (2005) 5407.
[5] T. Yuranova, G. Rincon, A. Bozzi, S. Parra, C. Pulgarin, P. Albers, J. Kiwi, J. Photochem. Photobiol. A: Chem. 161 (2003) 27–34.
[6] T. Yuranova, G. Rincon, C. Pulgarin, D. Laub, N. Xanthopoulos, H.-J. Mathieu, J. Kiwi, J. Photochem. Photobiol. A 181 (2006) 363–436.
[7] I. Mejía, G. Restrepo, J. Marín, R. Sanjinés, C. Pulgarín, E. Mielczarski, J. Mielczarski, J. Kiwi, ACS Appl. Mater. Interfaces 2 (2010) 230–235.
[8] J. Kiwi, C. Pulgarin, Catal. Today 151 (2010) 2–7.
[9] J.S. Yeon, Appl. Surf. Sci. 221 (2004) 281–287.
[10] L. Geranio, M. Heuberger, E. Nowack, Environ. Sci. Technol. 43 (2009) 8113–8118.
[11] D. Hegeman, M. Amberg, A. Ritter, M. Heuberger, Mater. Technol. 24 (2009) 41–45.
[12] D. Hegeman, M. Hossain, M. Balazs, Prog. Org. Coat. 58 (2007) 237–240.
[13] M. Radetic, V. Vodnik, S. Dimitrijevic, P. Jovancic, Z. Saponjic, J. Nedeljikocic, J. Polym. Adv. Technol. 19 (2008) 1816–1821.
[14] M. Kostic, N. Radic, M. Obradovic, S. Dimitrijevic, M. Kuraica, Plasma Process. Polym. 6 (2009) 58–67.
[15] U. Klueh, V. Wagner, S. Kelly, S. Johnson, A. Bryers, J. Biomed. Mater. Res. 53 (2000) 621–631.
[16] H.A. Foster, W.D. Sheel, P. Sheel, P. Evans, S. Varghese, N. Rutschke, M.H. Yates, J. Photochem. Photobiol. A 216 (2010) 283–289.
[17] M.S.P. Dunlop, P.C. Sheeran, A.J. Byrne, S.A.M. McMahon, A.M. Boyle, G.K. McGuigan, J. Photochem. Photobiol. A 216 (2010) 303–310.
[18] E. Rupp, T. Fitzgerald, N. Marion, V. Helget, S. Puumala, R. Anderson, D. Fey, Am. J. Infect. Control 32 (2004) 445–452.
[19] S. Ohashi, S. Saku, K. Yamaamoto, J. Oral Rehabil. 31 (2004) 364–369.
[20] AgION Technologies Inc., www.agion-tech.com.
[21] O. Baghriche, A.P. Ehiasarian, E. Kusiak, A.W. Morawski, C. Pulgarin, R. Sanjines, J. Kiwi, ACS Appl. Mater. Interfaces, submitted for publication.
[22] Z. Kertzman, J. Marchal, M. Suarez, M.H. Staia, P. Filip, P. Kohli, S.M. Aouadi, J. Biomed. Mater. Res. 84 (2008) 1061–1067.
[23] J.H. Hsieh, C.C. Tseng, Y.K. Chang, S.Y. Chang, W. Wu, Surf. Coat. Technol. 202 (2008) 5586–5589.
[24] P.C. Liu, J.H. Hsieh, C. Li, Y.K. Chang, C.C. Yang, Thin Solid Films 517 (2009) 4956–4960.
[25] H.L. Huang, Y.Y. Chang, M.-C. Lai, C.-R. Lin, C.-H. Lai, T.-M. Shieh, Surf. Coat. Technol. (2010), doi:10.1016/j.surfcoat.2010.07.096.
[26] J. Lin, J. Moore, W. Sproul, B. Mishra, Z. Wu, J. Wang, Surf. Coat. Technol. 204 (2010) 2230–2239.
[27] W.J. Mathews (Ed.), Epitaxial Growth, Part B, Ch 4: Nucleation of Thin Films, Academic Press, New York, 1975, pp. 382–486.
[28] J.P. Kelly, R.D. Arnell, Vacuum 56 (2000) 159–172 (and references therein).
[29] O.V. Krylov, Catalysis by Nonmetals, Academic Press, New York, 1980, p. 248.
[30] R. Houk, B. Jacobs, F. Gabay, N. Chang, D. Graham, S. House, I. Robertson, M. Allendorf, Nano Lett. 9 (2009) 3413–3418.
[31] A. Bozzi, T. Yuranova, E. Mielczarski, J. Mierzcalski, P.A. Buffat, P. Lais, J. Kiwi, Appl. Catal. B 42 (2003) 289–303.
[32] A. Bozzi, T. Yuranova, J. Mielczarski, J. Kiwi, New J. Chem. 28 (2004) 521–528.
[33] C.D. Wagner, W.M. Riggs, L.E. Davis, G.E. Mullenberg (Eds.), Handbook of X-ray Photoelectron Spectroscopy, Perkin-Elmer Corporation Physical Electronics Division, Minnesota, 1979.
[34] D.A. Shirley, Phys. Rev. B 5 (1972) 4709–4716.
[35] S. Chen, Y. Yin, D. Wang, Y. Lu, X. Wang, J. Cryst. Growth 282 (2005) 498–505 (and references therein).